JCTC Journal of Chemical Theory and Computation

Article

pubs.acs.org/JCTC

Hybrid Density Functionals for Clusters of Late Transition Metals: Assessing Energetic and Structural Properties

Thomas M. Soini,[†] Alexander Genest,[‡] Astrid Nikodem,[†] and Notker Rösch*[,†,‡]

[†]Department Chemie and Catalysis Research Center, Technische Universität München, 85747 Garching, Germany

[‡]Institute of High Performance Computing, Agency for Science, Technology and Research, 1 Fusionopolis Way, #16-16 Connexis, Singapore 138632

Supporting Information

ABSTRACT: We present the first application of hybrid density functional theory (DFT) methods to larger transition-metal clusters. To assess such functionals for this class of systems, we compare the performance of three modern hybrid DFT methods (PBE0, TPSSh, M06) and their semilocal counterparts (PBE, TPSS, M06L) regarding average bond distances and binding energies per atom for a series of octahedral model clusters M_n (M = Ni, Pd, Pt; n = 13, 38, 55, 79, 116). With application to large particles in mind, we extrapolated the results to their respective bulk limits and compared them to experimental values. In some cases, average nearest-neighbor distances are notably overestimated by the PBE0 and M06 hybrid functionals. Results on energies allow a grouping of the tested functionals into sets of similar behavior for the three metals studied. Among the methods examined, the TPSSh hybrid density functional shows the best overall performance.

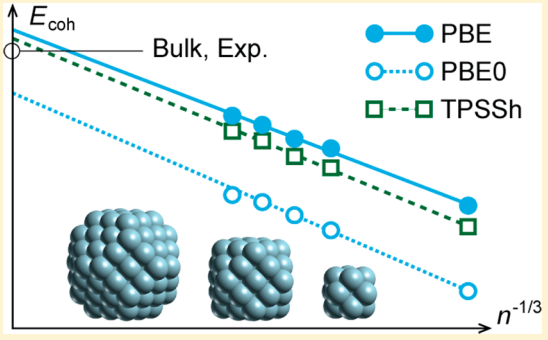

1. INTRODUCTION

Density functional theory[1] (DFT) within the Kohn−Sham (KS) framework[2] has seen many attempts and suggestions for improvement. Hybrid DFT, the admixture of exact exchange (EXX) to a semilocal exchange functional, is a very striking example of such an advance.[3,4] Initially, this scheme was empirically motivated;[3] theoretical justifications followed.[5−9] The B3LYP (hybrid) functional[10] soon emerged as the most widely applied DFT method.[11] With increasing popularity, it also became apparent that B3LYP offers limited accuracy for systems with bonds between transition-metal centers,[12−15] inferior to the computationally more efficient semilocal functionals that rely on the generalized gradient approximation (GGA). These problems were initially rationalized[16] by reference to the EXX term that partially substitutes the semilocal exchange part. While the latter implicitly accounts for static correlation,[16,17] the EXX term does not, because of its roots in a purely single-determinant theory. The implicit treatment of static correlation—hence, the effect of almost-equal contributions of several determinants to an electronic state—is therefore partially reduced in hybrid DFT methods, which may deteriorate their accuracy for metals, which are dominated by this effect.[17−20] However, a recent analysis[21] revealed the EXX term to be only a smaller source of error for transition metals.[13] Some missing exact constraints in the LYP correlation term and the exclusive parametrization of B3LYP on main group data[4,22] were found to contribute notably more.[18]

Newer hybrid DFT functionals try to avoid these latter deficiencies either by a less empirical construction[23] or a parametrization[24,25] that also accounts for data of small transition-metal compounds. This approach is exemplified by meta-GGA (mGGA) functionals whose additional functional dependency on the kinetic energy density promises even higher accuracy.[26,27] Nevertheless, the aforementioned static correlation error (SCE) remains present also in these new hybrid DFT methods. Of course, one must consider the clear advantages of hybrid DFT methods over semilocal functionals, particularly regarding reduced self-interaction artifacts.[19,24,28,29] This leads to the question whether the impact of the SCE is small enough in more recent hybrid DFT methods to admit a sufficiently accurate treatment of the electronic structure of transition-metal particles.

This situation motivated the present work on model clusters of late transition metals. In the spirit of earlier studies,[30,31] we employed model clusters[32,33] of various sizes to compare the performance of several (hybrid) DFT methods for structural, energetic, and electronic properties. Cluster scaling techniques permit one to extrapolate such results to their respective bulk limits and to compare these latter data to experiment.[34−39] We selected three popular semilocal density functionals and compared their results to their respective hybrid DFT counterparts. The PBE[40] GGA functional does not rely on any fitted parameters, and neither does its hybrid version, PBE0, whose (exact) exchange mixing factor of 0.25 is based on theoretical considerations.[23] The TPSS functional[26] is a

Received: August 3, 2014
Published: September 18, 2014

   dx.doi.org/10.1021/ct500703q | J. Chem. Theory Comput. 2014, 10, 4408−4416

nonempirical meta-GGA, whereas its hybrid version TPSSh[41] was obtained by optimizing its EXX prefactor, 0.10, on a set of experimental data. Finally, the functionals M06L[42] and M06[24,25] are examples for mGGA and hybrid mGGA functionals with a relatively large number of parameters that were assigned by comparison with several reference datasets. M06 has an EXX prefactor of 0.27, and M06L was obtained as its local reparameterization. Thus, in contrast to the other pairs of functionals examined in this work, M06L and M06 differ in the parameter values of their semilocal parts. While hybrid DFT methods with even larger EXX prefactors exist,[24] we will denote PBE0 and M06 in the following as functionals with a high fraction of exact exchange, to distinguish them from TPSSh.

2. THEORETICAL METHODS

2.1. Computational Details. All results were obtained by calculations with the linear combination of Gaussian-type orbital fitting-functions density functional (LCGTO-FF-DF) method.[43] The computations were carried out with the program package PARAGAUSS, version 4.0,[44] which recently was extended by options for exact exchange, hence, hybrid DFT functionals. Although PARAGAUSS includes its own electron repulsion integral routines, in the present study, an external, highly optimized implementation[45] was employed in combination with our recently developed dynamic load balancing library to achieve an efficient parallelization.[46]

We employed orbital basis sets of the type def2-TZVP,[47] which, for the elements Pd and Pt, include the corresponding Stuttgart−Dresden small-core pseudo-potentials.[48] For Ni, the def2-TZVP basis set describes all electrons. For the evaluation of the Hartree potential[43,49] the electronic charge density was approximated with an auxiliary basis set.[50,51] That standard set was extended by r^2-type functions,[43] but their effect on total energies was found to be negligible in preliminary tests on Pt_{13} and Pt_{38}, suggesting near completeness of the auxiliary basis set.

The semilocal exchange-correlation terms were evaluated by numerical integration. The corresponding grid was constructed as a superposition of spherical, atom-centered Lebedev-type grids.[52−54] The angular parts of these grids were locally exact for spherical harmonics with angular momentum up to $L = 29$; the radial part for Ni, Pd, and Pt consisted of 305, 315, and 305 radial shells, respectively. When assembling the exact exchange contribution to the Hamiltonian, a density-matrix-weighted Schwarz screening procedure[55] was applied with a tolerance of 10^{-10} a.u.

The self-consistent field (SCF) iterations were converged using the direct inversion of iterative subspace method,[56] until the relative change of the elements of the density matrix was below 5×10^{-6}. To facilitate the convergence, a fractional occupation number technique[43] was invoked using a Fermi-type level broadening. During geometry optimization, the energy range of the broadening function was reduced from 0.5 eV to finally 0.05 eV, to help selecting the energetically lowest electronic configuration. From a comparison with values extrapolated to integer occupations in an earlier study[57] (section 3.2), we find our results to be converged within ∼5 kJ/mol or less, with respect to the broadening parameter. Hence, we omitted an extrapolation to integer occupations.

All cluster structures were allowed to relax under O_h spatial symmetry constraints until the maximum gradient acting on each atomic center was below 10^{-5} a.u. For this task, the molecular-dynamics-based optimizer FIRE[58] was applied, available in the utility suite ParaTools.[59]

2.2. Cluster Models and Scaling Procedure. Suitable experimental references are hardly available for metal particles. Rather, comparison with calculated results often is restricted to the bulk material. To this end, we will exploit scaling laws based on cluster nuclearity.[34−36,60] To achieve good linear scaling behavior, we selected cluster models M_n (M = Ni, Pd, Pt) of close structural similarity with cut-outs of the corresponding fcc bulk metal, namely clusters of truncated cuboctahedral shape. As we are aiming for extrapolation to the bulk, this choice is preferable although more stable isomers likely exist.[37,61,62] Similarly, anisotropies and electronic situations with no relevance to the bulk are to be avoided in the present context. Therefore, we selected as models only clusters of O_h symmetry, of closed geometric shells and with a limited number of lower-coordinated atoms. We did not include octahedral clusters such as M_{19}, because of their low-coordinated corner atoms. Guided by these principles, one arrives at truncated octahedra, bounded by (111) and (001) facets, but without four-coordinated corner atoms. We considered cuboctahedral cluster models M_n with up to 3 shells of atoms, n = 13, 38, 55, 79, and 116 (Figure 1). M_{13}, M_{55}, and M_{79} are atom-centered clusters, and M_{38} and M_{116} have an octahedron M_6 as central moiety.

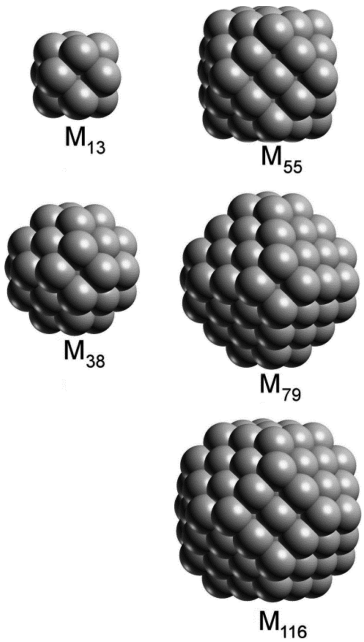

Figure 1. Sketches of the cluster models M_n (M = Pt, Pd, and Ni; n = 13, 38, 55, 79, and 116).

In analogy to the geometric features of the cluster models, one may also strive for unifying features of the electronic structures of the clusters in a series to be used for extrapolation. However, constraining the magnetic moments per atom of the cluster models to the corresponding bulk values (i.e., zero for Pt and Pd, 0.616 for Ni) yields variations of up to 5 pm for the extrapolated nearest-neighbor average distances and 30 kJ/mol for the cohesive energies. This is to be expected because at least the smaller model clusters still behave as molecular entities. Furthermore, the differences were found larger for the results of hybrid DFT calculations, because of their increased band gaps that enhance the aforementioned molecular behavior. Therefore, only results of unrestricted Kohn−Sham calculations will be discussed in the following. Results from spin-restricted

dx.doi.org/10.1021/ct500703q | J. Chem. Theory Comput. 2014, 10, 4408−4416

Table 1. Extrapolated Cluster Values of Average Nearest-Neighbor Distances (d_{av}) Obtained for Bulk Metals Ni, Pd, and Pt from Calculations with the Six Functionals Examined (Also Shown Are the Corresponding Values of the Fitted Slopes (k_d) and the Coefficients of Determination R^2, as Well as Experimental Values)

		PBE	PBE0	TPSS	TPSSh	M06L	M06	exp
Ni	d_{av} (pm)	252.8	258.7	251.1	252.0	253.3	258.9	249[a]
	k_d	−13.6	−23.4	−11.8	−12.1	−12.4	−23.1	
	R^2	0.946	0.946	0.944	0.950	0.959	0.948	
Pd	d_{av} (pm)	279.8	280.8	276.7	276.9	279.3	288.1	275[b]
	k_d	−23.9	−30.0	−22.0	−23.0	−20.4	−31.9	
	R^2	0.984	0.993	0.984	0.971	0.969	0.935	
Pt	d_{av} (pm)	283.9	281.6	281.9	281.0	284.6	290.9	277[c]
	k_d	−33.9	−31.6	−32.5	−31.8	−31.4	−37.4	
	R^2	0.987	0.926	0.988	0.984	0.989	0.996	

[a]Data taken from ref 67. [b]Data taken from ref 68. [c]Data taken from ref 69.

calculations are presented and briefly discussed in the Supporting Information (SI) (see Section S1).

The calculations of atomic species, required for calculating cohesive energies, were carried out in C_{2v} symmetry to admit a localized occupation of all valence shells. The resulting atomic electron configurations were found to be $3d^9 4s^1$ for Ni, $4d^{10}$ for Pd, and $5d^9 6s^1$ for Pt. The latter two results match the corresponding experimental findings.[63] In the case of Ni, the experimental configuration $3d^8 4s^2$ is known to be preferred bceause of a spin−orbit interaction[64] that is not considered here.

The extrapolation to the bulk limit exploits the finding that many properties $X(n)$ of metal clusters M_n were found to scale quite nicely with $n^{-1/3}$ in linear fashion:[31,34−36,60,65]

$$X(n) = k_X n^{-1/3} + X_\infty \quad (1)$$

With a least-squares fit of the calculated data $X(n)$ to this relationship, one is able to identify the slope k_X as well as the predicted bulk limit X_∞ for $n \rightarrow \infty$.[31,34−36,60,65] This relationship is expected to hold for sufficiently large cluster sizes n, from a minimum n_{scal} onward, for quantities that scale with the surface-to-volume ratio of the particles, or the inverse of the effective particle radius or $n^{-1/3}$.[34−36,60] The specific value of n_{scal} is dependent, of course, on the properties and the systems examined.[33,65,66]

3. RESULTS AND DISCUSSION

3.1. Average Bond Length. Average nearest-neighbor distances d_{av} of moderately large metal clusters are known to increase smoothly with cluster size.[31,35,36,38] This behavior reflects the trend to decreasing bond distances when the average coordination number decreases because larger clusters comprise a smaller fraction of surface atoms with lower coordination numbers, hence featuring stronger interactions with their neighboring atoms.[35,36] Apart from reflecting such physical variations, these changes in geometry also provide first insight into the quality of the extrapolation procedure (Table 1). Results for individual clusters are collected in Table S3 of the SI, while Figure 2 shows the corresponding linear function (eq 1) on the example of Pt. A graphical comparison of the data for all three metals and the corresponding fitting functions are provided as Supporting Information (Figure S1).

As expected, the d_{av} values increase with the nuclearity of the cluster models. We compare the PBE estimate for Pd also to the corresponding results of a recent all-electron cluster scaling

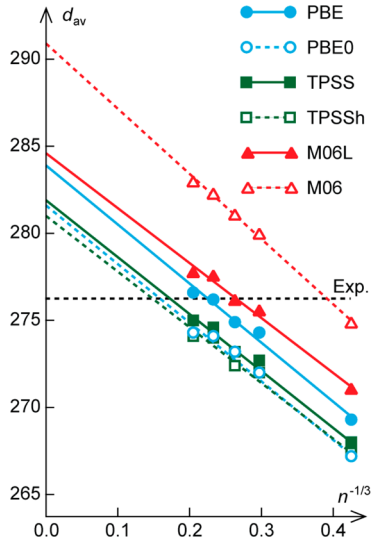

Figure 2. Average nearest-neighbor distances d_{av} (pm) calculated for the model clusters Pt_n together with the fitted trend line linear in $n^{-1/3}$.

study,[31] which agree extremely well, within 0.1 pm. For most exchange-correlation approximations, the coefficients of determination (R^2) increase along the series Ni < Pd < Pt; PBE0 represents an exception, because of its higher R^2 value of 0.993 for Pd. Otherwise, R^2 values typically are ∼0.95 for Ni, ∼0.98 for Pd, and generally even higher for Pt. From these results, one concludes that extrapolation of the average bond lengths to the corresponding bulk limits is generally well-justified.

The bulk limits d_{av} can generally be ordered as follows (see Table 1): d(TPSS) ≈ d(TPSSh) < d(PBE) ≈ d(M06L) < d(PBE0) ≈ d(M06). Only for Pt, PBE0 yields a comparatively low limit for d_{av}, because of minor outliers in this data series. Comparing the semilocal DFT methods with their hybrid DFT counterparts, one finds that the functionals PBE0 and M06 (i.e., the functionals with a high fraction of single-determinant exchange) mostly overestimate bonds lengths. The extrapolated results d_{av}(PBE0) are by 1.0 pm (Pd) and 5.9 pm (Ni) larger than the corresponding PBE values. Compared to M06L, the M06 method yields extrapolated bulk distances that are higher−by 5.6 pm for Ni, 6.0 pm for Pd, and 5.2 pm for Pt. Only the aforementioned PBE0 result for Pt is 2.1 pm smaller than the corresponding PBE result. This significant impact of the exact exchange term on structural properties can be

dx.doi.org/10.1021/ct500703q | J. Chem. Theory Comput. 2014, 10, 4408−4416

Table 2. Extrapolated Cluster Values of the Cohesive Energy E_{coh} per Atom Obtained for Bulk Metals Ni, Pd, and Pt from Calculations with the Six Functionals Examined (Also Shown Are the Corresponding Values of the Fitted Slopes (k_E) and the Coefficients of Determination (R^2), as Well as Experimental Values)

		PBE	PBE0	TPSS	TPSSh	M06L	M06	exp
Ni	E_{coh} (kJ/mol)	444.6	303.6	459.4	393.5	462.2	347.8	428[a]
	k_E (kJ/mol)	−405.5	−304.3	−452.6	−409.6	−491.4	−387.8	
	R^2	0.993	0.994	0.994	0.996	0.998	0.981	
Pd	E_{coh} (kJ/mol)	395.9	337.1	425.0	387.8	440.3	315.4	376[b]
	k_E (kJ/mol)	−381.3	−431.7	−427.5	−410.2	−478.7	−370.7	
	R^2	0.996	1.000	0.997	0.998	0.998	0.999	
Pt	E_{coh} (kJ/mol)	555.9	494.5	580.1	546.8	579.9	487.1	563[b]
	k_E (kJ/mol)	−512.1	−530.3	−566.0	−547.5	−583.6	−470.0	
	R^2	0.995	0.991	0.995	0.996	0.997	0.995	

[a]Data taken from ref 74 [b]Data taken from refs 72 and 73.

rationalized by the fact that hybrid DFT functionals prefer other electronic states than semilocal functionals, as will be discussed in section 3.3. These states subsequently lead to different structures. Compared to all other methods, the slopes (k_d) of the linear trend lines of PBE0 and M06 for Ni and Pd are notably more negative (see Table 1). The Pd_n structures obtained with PBE0 are less expanded than the corresponding PBE and M06L geometries, so that the overestimation of the bulk limit results entirely from the steeper slope. The situation is different for TPSSh where the EXX contribution is smaller. This functional yields extrapolated d_{av} values that are very similar to the corresponding TPSS results, with differences of <1 pm and linear trend lines of almost the same slopes.

All DFT methods examined overestimate the experimental nearest-neighbor distances of the metal bulk. The TPSS result for bulk Ni, 251.1 pm, is closest to the experimental reference, 249 pm.[67] The TPSSh functional yields a slightly larger value, 252.0 pm, which is the second-most accurate result for Ni. For Pd, the extrapolated d_{av} value, 276.9 pm, of TPSSh is barely larger than the TPSS result, 276.7 pm, and is rather close to the experimental reference, 275 pm.[68] Indeed, the TPSSh functional does not only yield d_{av} extrapolations close to those obtained with TPSS, but, in the case of Pt, also a slightly better estimate, 281.0 pm, which agrees best with the experimental reference, 277 pm.[69] Interestingly, the analogous PBE0 result for Pt, 281.6 pm, represents the second-best estimate for the experimental bulk value, deviating by 4.6 pm, closely followed by the TPSS result, 281.9 pm. The PBE and M06L functionals, with 283.9 and 284.6 pm, respectively, are somewhat less accurate for Pt, while M06, with 290.9 pm, notably overestimates the experimental value of Pt.

The two semilocal functionals PBE and M06L also yield similar results for the other two metals: 252.8 and 253.3 pm for Ni; 279.8 and 279.3 pm for Pd. The good accuracy of the PBE0 functional noted for Pt does not carry over to Pd, where the nearest-neighbor distance of the bulk is estimated at 280.8 pm. Thus, the corresponding deviation of 5.8 pm is significantly higher than those of TPSS and TPSSh. For Ni, the situation is even worse; the extrapolated bulk value is 258.7 pm, close to the corresponding M06 result. Both values overestimate the experiment by 10 pm. The M06 functional shows the same overestimations also for the other two metals, yielding 288.1 pm for Pd (13 pm above the experimental value) and 290.9 pm for Pt (14 pm above) (see Table 1).

Therefore, except for Pt, we are unable to confirm a good performance of PBE0, as reported for the bulk metals in recent plane-wave studies.[21,70] Although the corresponding d_{av} values are mostly smaller than the present results, the overall agreement between the two datasets still seems reasonable.

3.2. Cohesive Energy. The cohesive energy E_{coh} per atom of a cluster M_n is determined from the total energies $E_{tot}(M_n)$ of the cluster and $E_{tot}(M_1)$ of the corresponding atomic species:

$$E_{coh}(M_n) = E_{tot}(M_1) - E_{tot}(M_n)/n \quad (2)$$

The values $E_{coh}(M_n)$ are expected to grow with cluster size n, because the fraction of low coordinated surface atoms decreases as the surface-to-volume ratio decreases, i.e., with $n^{-1/3}$. Table 2 provides the resulting trend lines (eq 1) from fitting calculated results (eq 2), as well as corresponding experimental reference values. For the latter case, temperature and zero point energy (ZPE) corrections are below 4 kJ/mol and, thus, are neglected.[70,71] The cohesive energies obtained for the individual cluster models are listed in Table S4 of the SI. These latter values indeed show the expected growth, as is also shown in Figure 3, with regard to the example of the Pt_n clusters. In Figure S2 of the SI, we compare results for all three metals.

Before discussing the E_{coh} bulk limits obtained with the various functionals, we compare the present PBE extrapolation for Pd, 395.9 kJ/mol, with the corresponding value, 375.6 kJ/mol, obtained in an earlier study.[31] Recently, that deviation of 20 kJ/mol has been traced[57] to the use of pseudo-potentials.[48] Despite the different cluster series employed, the PBE/def2-TZVP results in both studies agree within a few kJ/mol. Compared to recent plane-wave results for the bulk materials,[70] we obtain somewhat smaller E_{coh} values for Ni and always larger bulk extrapolations for the other two metals. However, the deviations are consistent with those found earlier[57] and likely may be due to methodological differences, namely, different treatment of the atomic systems, the pseudo-potentials employed here, and the plane-wave projector-augmented wave approach to atomic cores invoked in plane-wave calculations.

Because of the considerably larger range of energy values, the R^2 coefficients of the cohesive energy trend lines are consistently larger than in the case of the average nearest-neighbor distances; see Tables 1 and 2. Indeed, for E_{coh}, the R^2 coefficients are always above 0.99, with one exception, for the

dx.doi.org/10.1021/ct500703q | J. Chem. Theory Comput. 2014, 10, 4408−4416

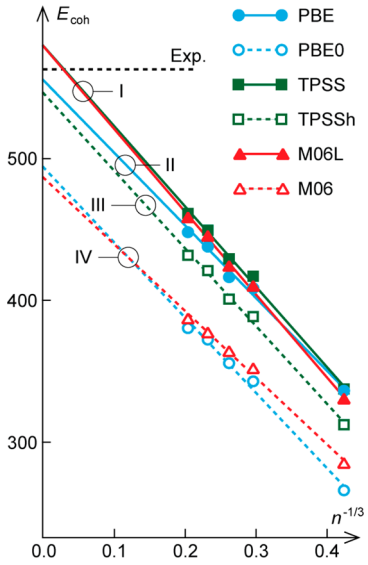

Figure 3. Cohesive energies E_{coh} (kJ/mol) per atom calculated for the model clusters Pt_n, together with the fitted trend line linear in $n^{-1/3}$. The assignment to the various groups (see text) is indicated by circles: Group I, TPSS and M06L; Group II, PBE; Group III, TPSSh; and Group IV, PBE0 and M06.

M06 series of Ni_n clusters, where one determines a value of R^2 = 0.97 (see Table 2).

Comparing results of related semilocal and hybrid functionals, it certainly is most striking that the cohesive energies are considerably reduced when exact exchange is included. As judged by the extrapolated estimates for the bulk cohesive energies, determined for the pairs PBE/PBE0 and TPSS/TPSSh, this reduction is notably higher for Ni than for Pd and Pt. For the latter two elements, this effect is of comparable size. The changes are about twice as large for PBE/PBE0 than for TPSS/TPSSh. These effects correlate approximately with the weight of the corresponding EEX terms, 0.25 in PBE0[23] and 0.10 in TPSSh.[41] While TPSSh provides accurate structures, despite somewhat underestimated bond strengths for Ni and Pt, the quality of structural results obtained with PBE0 breaks down for Ni, as indicated by the strongly reduced E_{coh} value, compared to PBE. It may seem counterintuitive that a hybrid DFT method and its semilocal counterpart can yield similar metal−metal distances, but quite different cohesive energies. Yet, such type of results have also been reported in a recent plane-wave study.[21] The situation is different for the M06L/M06 pair where bond elongation always correlates with a reduction of the bond strength. Both of these aspects, bond elongation and bond strength, are largest for Pd, and smallest, but still comparable, for Pt; most likely, they originate from the different semilocal terms of M06L and M06.

Examining the results in Table 2 and the plots of the linear trend lines in more detail (see Figure 3, as well as Figure S2 in the SI), we classify the assessed functionals into four groups.

Group I includes the pure meta-GGA functionals TPSS and M06L, which, for all three metals, yield rather comparable estimates of the extrapolated cohesive energies that are also larger than the values from the other four functionals. For Pt, the bulk cohesive energies are estimated at 580.1 kJ/mol for TPSS and 579.9 kJ/mol for M06L; these values are ∼17 kJ/mol larger than the experimental reference, 563 kJ/mol.[72,73] The cohesive energies of the other two metals are somewhat more overestimated. The results for the extrapolated cohesive energy of Ni amount to 459.4 kJ/mol (TPSS) and 462.2 kJ/mol (M06L), overestimating the experimental reference, 428 kJ/mol,[74] by ∼30 kJ/mol. For Pd, the estimated bulk limits of E_{coh}, 425.0 kJ/mol (TPSS) and 440.3 kJ/mol (M06L), surpass the experimental result, 376 kJ/mol,[72,73] by 49 and 64 kJ/mol, respectively. Thus, the exceptionally good performance of TPSS for metallic systems reported in other studies[27,75] does not seem to apply for the larger Pd model clusters examined here. The rather large deviation between the experimental cohesive energy reference of Pd and the corresponding M06L result may be related to specific deficiencies of this functional, noted previously for smaller Pd clusters.[30]

Group II comprises the pure GGA functional PBE whose estimates of the cohesive energy are always lower than the corresponding ones in Group I. PBE overestimates the references for Ni and Pd only slightly, while underestimating in the case of Pt. For Ni, this functional estimates the cohesive energy at 444.6 kJ/mol. With a deviation of ∼17 kJ/mol, PBE shows the best accuracy of all tested methods for the cohesive energy of Ni; the result compares well to that of a similar cluster study.[76] The PBE result for Pd is 395.9 kJ/mol; it is ∼20 kJ/mol larger than the experimental value. For Pt, the PBE functional yields an extrapolated cohesive energy of 555.9 kJ/mol, which is again the most accurate estimate, with a deviation of only 7.1 kJ/mol.

The hybrid DFT method TPSSh with its low exact exchange fraction forms Group III. For Ni, Pd, and Pt, it yields bulk cohesive energies of 393.5, 387.8, and 546.8 kJ/mol, respectively. The Pd result represents the best match among the six functionals (12 kJ/mol deviation), while the estimates for Pt and Ni are still among the most accurate, with deviations comparable to those of the Group I functionals.

Finally, Group IV includes the hybrid DFT methods PBE0 and M06, which yield the lowest extrapolated values of the cohesive energy and, in many cases, the worst accuracy, because of a strong underestimation of the experimental reference values (see Table 2). The Pd bulk limits—337.1 kJ/mol (PBE0) and 315.4 kJ/mol (M06), deviate from the experiment result even more than M06L, by 39 and 61 kJ/mol, respectively. For Pt, PBE0 and M06 yield rather similar extrapolations, 494.5 and 487.1 kJ/mol, respectively, with deviations of ∼70 kJ/mol. The M06 bulk limit of the cohesive energy for Ni is 347.8 kJ/mol, with an error of 80 kJ/mol, while the corresponding PBE0 result, 303.6 kJ/mol, is ∼125 kJ/mol below the reference value. Thus, one notes a somewhat erratic behavior of the functionals with large fractions of exact exchange, especially in the case of Ni. These errors are likely related to the static correlation error, which is most pronounced for these DFT approximations.[77,78]

3.3. Electronic Properties. Now, we will discuss several aspects of the electronic structure of M_n species that often are dominated by just a few orbitals. As a consequence, such quantities show only a late onset n_{scal} of their scalable regime.[65,79]

We begin with a discussion of the vertical ionization potential (IP) (Φ_{IP}) and the electron affinity (EA) (Φ_{EA}) which, for larger metal clusters, can be well-described by the well-known droplet model.[60] To minimize the Coulombic repulsion, the charge distribution in the resulting ionic species takes on an increasingly extended form. Therefore, Φ_{IP} decreases and Φ_{EA} increases to the common bulk limit, the work function Φ. These interpretations of IP and EA results have extensively been discussed in previous cluster scaling studies.[34,60,80] In the

dx.doi.org/10.1021/ct500703q | J. Chem. Theory Comput. 2014, 10, 4408−4416

Table 3. Extrapolated Vertical Ionization Potentials Φ_{IP}, Vertical Electron Affinities Φ_{EA} of Clusters and Their Difference $\Delta\Phi = \Phi_{IP} - \Phi_{EA}$ of Cluster Results Obtained for Bulk Metals Ni, Pd and Pt from Calculations with the Six Functionals Examined (Also Shown Are the Corresponding Values[a] of the Fitted Slopes (k_{IP} and k_{EA}), as Well as the Coefficients of Determination (R^2) and the Experimental Values)

		PBE	PBE0	TPSS	TPSSh	M06L	M06	exp
Ni	Φ_{IP} (eV)	4.63	2.02	4.64	3.10	2.72	3.80	5.04−5.35[b]
	k_{IP} (eV)	3.23	11.49	2.71	7.46	7.98	5.96	
	R^2	0.996	0.838	0.489	0.934	0.172	0.510	
Pd	Φ_{IP} (eV)	4.72	4.15	4.56	4.23	4.75	6.32	5.22−5.60[b]
	k_{IP} (eV)	4.72	7.26	4.84	5.90	3.55	0.26	
	R^2	0.756	0.589	0.722	0.759	0.752	0.017	
Pt	Φ_{IP} (eV)	5.54	5.30	5.40	4.95	5.25	5.70	5.12−5.93[b]
	k_{IP} (eV)	3.71	4.56	3.94	6.03	3.45	4.88	
	R^2	0.820	0.619	0.849	0.868	0.807	0.900	
Ni	Φ_{EA} (eV)	4.72	3.03	4.45	4.20	3.99	6.31	5.04−5.35[b]
	k_{EA} (eV)	−6.14	−1.66	−5.81	−6.03	−4.60	−13.16	
	R^2	0.944	0.141	0.876	0.899	0.961	0.919	
Pd	Φ_{EA} (eV)	4.74	4.73	4.67	4.72	4.61	5.67	5.22−5.60[b]
	k_{EA} (eV)	−4.12	−5.30	−4.46	−5.11	−4.52	−7.29	
	R^2	0.788	0.378	0.804	0.771	0.910	0.900	
Pt	Φ_{EA} (eV)	5.35	4.88	5.23	5.80	5.16	5.97	5.12−5.93[b]
	k_{EA} (eV)	−4.64	−3.23	−4.13	−6.51	−4.70	−5.29	
	R^2	0.830	0.090	0.779	0.783	0.970	0.439	
Ni	$\Delta\Phi$ (eV)	−0.90	−1.01	0.18	−1.09	−1.28	−2.51	0.00[c]
Pd	$\Delta\Phi$ (eV)	−0.02	−0.58	−0.11	−0.49	0.14	0.66	0.00[c]
Pt	$\Delta\Phi$ (eV)	0.19	0.42	0.17	−0.85	0.09	−0.28	0.00[c]

[a]The calculated results for M_{13} were not used in the fitting procedures. [b]Data taken from refs 81−83. [c]Φ_{IP} and Φ_{EA} assume identical values of the work function in the bulk limit.

present work, we calculated these quantities within the ΔSCF approximation:

$$\Phi_{IP}(M_n) = E_{tot}(M_n^+) - E_{tot}(M_n)$$
$$\Phi_{EA}(M_n) = E_{tot}(M_n) - E_{tot}(M_n^-) \quad (3)$$

Table 3 provides the extrapolated results and the corresponding fitting parameters, while the results calculated for the individual cluster models are given in Tables S5 and S6 in the SI. The values of the M_{13} clusters were found to exhibit strongly molecular characteristics and, hence, were excluded from these extrapolations. Compared to the extrapolations discussed in the previous sections, it is most striking that the IP and EA series have significantly lower R^2 values. For some series of results, mostly originating from PBE0 and M06 calculations, $R^2 \ll 0.75$; thus, the results hardly scale at all in the set of clusters under study. We first will discuss the smoothly extrapolating data, before addressing the lack of scalability in the other cases.

For Pt, the IP extrapolations of PBE (5.54 eV), TPSS (5.40 eV), M06L (5.25 eV), and M06 results (5.70 eV) are all within the range of experimental data, 5.12−5.93 eV, because of measurements on crystalline surfaces of several orientations.[81−83] The TPSSh result, 4.95 eV, slightly underestimates the work function. The EA extrapolations of PBE, TPSS, TPSSh, and M06L all also agree with the reference range. For Pd, the IP and EA series of these four functionals underestimate the work function by ∼0.5−1.0 eV, while the Φ_{EA} series of M06 overestimates the reference range by only a small amount. For Ni, only the IP results of PBE, PBE0, and TPSSh exhibit reasonable scaling behavior. However, the TPSSh extrapolation underestimates the reference by 1.9 eV and the PBE0 result does so by more than 3 eV. Most Ni EA series have a significantly better scaling behavior, underestimating the experiment somewhat less, by, at most, ∼1 eV in the case of M06L. Only the M06 results yield a significantly higher bulk limit, overestimating the reference range by ∼1 eV. Extrapolation of the differences $\Delta\Phi(M_n) = \Phi_{IP}(M_n) - \Phi_{EA}(M_n)$ allows one to check whether a zero band gap is obtained in the bulk limit (Table 3). Here, the errors are largest for Ni, where only TPSS provides a reasonable estimate, 0.18 eV, while the other methods yield ΔΦ limits from −0.9 eV (PBE) to −2.5 eV (M06). For Pd and Pt, the extrapolated values are closer to 0 eV, while results of semilocal functionals deviate by <0.2 eV from the theoretical limit. Indeed, all hybrid functionals yield larger ΔΦ values than their corresponding semilocal counterparts.

Now, we turn to discussing reasons for the stronger scattering of IP and EA extrapolations compared to other properties. For systems with a small HOMO−LUMO gap, the employed level broadening formalism involves many orbitals in the ionization process. However, for smaller clusters and/or hybrid DFT calculations, the HOMO−LUMO gap is large and single orbitals dominate the IP and EA energies. The latter systems seem to be associated with the outliers whenever one of the dominating levels happens to be symmetry-degenerate

dx.doi.org/10.1021/ct500703q | J. Chem. Theory Comput. 2014, 10, 4408−4416

(*e*- or *t*-type) as well as partially occupied in either the ionic system or the neutral system. Since this degeneracy arises directly from the symmetry constraints imposed on the model clusters, this clearly represents a drawback of the employed strategy that relies on models of O_h symmetry. The high symmetry, however, does not only reflect the electronic structure in the fcc bulk limit, but is also essential for converging the electronic structure of larger metallic systems.

Compared to earlier all-electron PBE results for Pd,[31] the present extrapolations are lower by 0.33 eV (IP) and 0.15 eV (EA). These differences can be attributed to the stronger level broadening employed in that earlier study as well as to the slightly different choice of cluster models, used in the extrapolation series (Pd_{147} instead of Pd_{116}). The present extrapolation $\Delta\Phi$ is by 0.14 eV closer to the theoretical limit of 0.0 eV.

The fact that level broadening can affect the results to such an extent warrants further discussion and brings us back to the already-mentioned static correlation error. Indeed, besides the LDA exchange term, the level broadening formalism also is known to account implicitly for this correlation effect.[84−86] In this context, one may identify the following combination of factors required for an implicit description of the interaction between multiple determinants. (i) A sufficient amount of LDA exchange leads to (ii) a vanishing band gap in the case of larger metallic system. This, in turn, should yield (iii) a nonzero density of states (DOS) around the Fermi level and therefore to orbitals accessible to a fractional occupation by (iv) a level broadening formalism. The Kohn−Sham DFT method is a purely single-determinant based formalism and does not provide any measure for static correlation, so that the factors just listed represent only a rough guideline. However, they seem to suffice for rationalizing the different behavior of hybrid DFT methods, compared to semilocal functionals, as diagnosed in the present study. To this end, we examined the number of orbitals I_{DOS} within a certain energy interval around the center of the HOMO−LUMO gap (or the Fermi energy (ε_F)). For an extended system, this count turns into an integral over the DOS. We chose the ranges $[\varepsilon_F - 0.5\ eV, \varepsilon_F]$ (count of occupied level) and $[\varepsilon_F - 0.5\ eV, \varepsilon_F + 0.5\ eV]$ (total orbital count), referring to the resulting level counts by I^{occ}_{DOS} and I^{tot}_{DOS}, respectively; see Figure 4 for the values I^{occ}_{DOS} and I^{tot}_{DOS} for the Pt_n model clusters calculated with the functionals PBE, PBE0, and TPSSh.

Aside from minor deviations for smaller clusters, the number of orbitals around the Fermi level increases, as expected, with the system size. Both, I^{occ}_{DOS} and I^{tot}_{DOS} are highest for PBE and lowest for PBE0 (see Figure 4). In the latter case, I^{occ}_{DOS} remains close to zero, even at cluster sizes of $n = 116$. Also, M06 was found to yield comparatively low values, while the mGGA functionals behave quite similar to PBE. Surprisingly, the I_{DOS} values of the low EXX hybrid functional TPSSh are smaller than those of semilocal DFT methods, but still are fairly large. TPSSh shows also reasonably large I^{occ}_{DOS} and I^{tot}_{DOS} values for Pd and Ni, whereas the values from PBE0 and M06 calculations also remain very low in these cases. This can be attributed to the different amount of the EXX contribution. The EXX term in TPSSh seems small enough to admit orbitals near the HOMO−LUMO gap, which obviously is necessary for adequately modeling a metallic system, as implied by the extrapolation to very large metal particles. Indeed, the Hartree−Fock method severely fails for metal systems, because it produces a depleted DOS near ε_F.[87] As a consequence, hybrid

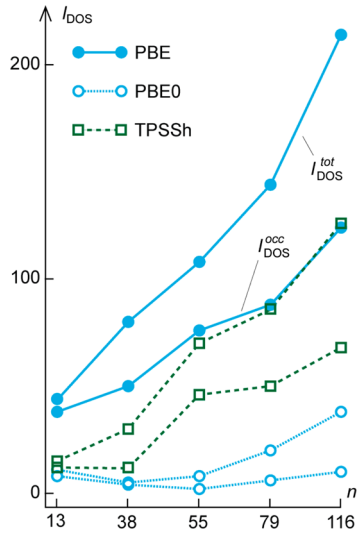

Figure 4. Number of occupied orbitals, I^{occ}_{DOS} (lower line), and total number of orbitals, I^{tot}_{DOS} (upper line), of model clusters Pt_n in the interval up to 0.5 eV from the center of the HOMO−LUMO gap. Trend lines are shown to guide the eye, marked for the PBE values. See text for details.

DFT methods with some amount of EXX also can be expected to behave similarly, which allows one to rationalize the failure observed for PBE0 and M06. However, we take the above findings as a strong indication that the TPSSh functional, despite its 10% EXX term, yields a reasonable representation of the electronic structure of the examined metal cluster models. As a consequence, this may rationalize the good performance of TPSSh when calculating bond lengths and cohesive energies of metal particles.

Finally, some comments on the calculated magnetic moment per atom μ_a (see Table S7 in the SI). Small transition-metal clusters are often magnetic, even for elements that are nonmagnetic in the bulk limit.[30,65,79] Furthermore, the magnetic moment can oscillate for cluster sizes of up to 700 atoms,[65,79] which prevents an extrapolation of this quantity for the systems under study. For larger clusters, the EXX term, added directly in the functionals PBE0 and TPSSh, mostly leads to higher μ_a values, compared to semilocal counterparts. This propensity for high-spin states was also obtained in a previous study.[29] In contrast, with the functional M06L, primarily, higher μ_a values were calculated than with the hybrid functional M06. In this context, also recall earlier findings for M06L.[30] This systematic disparity between M06 and M06L may again be related to the separate parametrizations of the semilocal and the hybrid variant of the exchange functional.

4. CONCLUSION

Not unexpectedly, the exact exchange term in hybrid density functional theory (DFT) methods is found to have a significant impact on all examined physical properties of the Group 10 transition-metal clusters. These methods generally prefer high-spin configurations and lead to weakened metallic bonds. The direct inclusion of an EXX contribution with a prefactor of more than 0.2, as in the case of PBE0, leads to erratic behavior of all quantities, except for some nearest-neighbor distances. The same holds for the M06 functional, which, together with its semilocal counterpart M06L, also seems to suffer from empirical aspects of its construction.

The situation is different for the hybrid functional TPSSh, whose significantly smaller exact exchange contribution seems to offer a good compromise between semilocal and hybrid density functionals in the case of transition-metal clusters. The structural quantities obtained with this functional are found to be the most accurate among all examined functionals. Furthermore, the functional performs also quite well for cohesive energies. Regarding electronic properties, the accuracy of its results is lower than those of other functionals, but all properties were calculated at adequate accuracy. We rationalized the surprisingly solid performance, compared to the other two hybrid DFT methods, by examining the behavior of the density of states around the HOMO−LUMO gap. In the case of TPSSh, the density of states (DOS) in this energy range still seems large enough to allow an implicit inclusion of static correlation interactions. Self-interaction corrections and a description of static correlation often are counteracting each other in exchange-correlation approximations,[18] but the TPSSh functional seems to offer a reasonable compromise between these two aspects, thus providing a useful description of the electronic structure of large transition-metal particles.

Overall, the hybrid meta-GGA functional TPSSh seems to be at least on par with the semilocal GGA functional PBE for the studied properties of the Group 10 transition-metal clusters. Therefore, it seems attractive to apply this functional to surface science problems and transition-metal catalysis, where the advantages of hybrid DFT may be important.

■ ASSOCIATED CONTENT

Supporting Information

All results of the individual systems, used for the cluster scaling extrapolations, are provided in the Supporting Information. Tables S1 and S2 contain the results $d_{av}(M_n)$ and $E_{coh}(M_n)$, respectively, that were obtained by restricting the magnetic moment to the bulk limit of the metals studied. Tables S3−S6 contain the values $d_{av}(M_n)$, $E_{coh}(M_n)$, $\Phi_{IP}(M_n)$, and $\Phi_{EA}(M_n)$, respectively, from the unrestricted calculations. Figures S1 and S2 depict the extrapolation plots of the latter data for $d_{av}(M_n)$ and $E_{coh}(M_n)$, respectively. Table S7 provides the magnetic moments per atom obtained for the individual clusters. This material is available free of charge via the Internet at http://pubs.acs.org.

■ AUTHOR INFORMATION

Corresponding Author

*E-mail: roesch@mytum.de.

Notes

The authors declare no competing financial interest.

■ ACKNOWLEDGMENTS

We thank Dr. Sven Krüger for valuable discussions. T.M.S. and A.N. are grateful for financial support of the International Graduate School of Science and Engineering (IGSSE) of Technische Universität München. The authors also acknowledge a generous grant of computing resources by the Gauss Centre for Supercomputing (www.gauss-centre.eu), provided on the SuperMUC platform of Leibniz Supercomputing Centre Garching (www.lrz.de).

■ REFERENCES

(1) Hohenberg, P.; Kohn, W. *Phys. Rev.* **1964**, *136*, B864−B871.
(2) Kohn, W.; Sham, L. *Phys. Rev.* **1965**, *140*, A1133−A1138.
(3) Becke, A. D. *J. Chem. Phys.* **1993**, *98*, 1372−1377.
(4) Becke, A. D. *J. Chem. Phys.* **1993**, *98*, 5648−5652.
(5) Talman, J. D.; Shadwick, W. F. *Phys. Rev. A* **1976**, *14*, 36−40.
(6) Harris, J. *Phys. Rev. A* **1984**, *29*, 1648−1659.
(7) Burke, K.; Ernzerhof, M.; Perdew, J. P. *J. Chem. Phys.* **1996**, *105*, 9982−9985.
(8) Seidl, A.; Görling, A.; Vogl, P.; Majewski, J. A.; Levy, M. *Phys. Rev. B* **1996**, *53*, 3764−3774.
(9) Burke, K.; Ernzerhof, M.; Perdew, J. P. *Chem. Phys. Lett.* **1997**, *265*, 115−120.
(10) Stephens, P. J.; Devlin, F. J.; Chabalowski, C. F.; Frisch, M. J. *J. Phys. Chem.* **1994**, *98*, 11623−11627.
(11) Sousa, S. F.; Fernandes, P. A.; Ramos, M. J. *J. Phys. Chem. A* **2007**, *111*, 10439−10452.
(12) Reiher, M.; Salomon, O.; Hess, B. A. *Theor. Chem. Acc.* **2001**, *107*, 48−55.
(13) Schultz, N.; Zhao, Y.; Truhlar, D. G. *J. Phys. Chem. A* **2005**, *109*, 4388−4403.
(14) Schultz, N.; Zhao, Y.; Truhlar, D. G. *J. Phys. Chem. A* **2005**, *109*, 11127−11143.
(15) Harvey, J. N. *Annu. Rep. Prog. Chem., Sect. C* **2006**, *102*, 203−226.
(16) Handy, N. C.; Cohen, A. J. *Mol. Phys.* **2001**, *99*, 403−412.
(17) Cremer, D. *Mol. Phys.* **2001**, *99*, 1899−1940.
(18) Polo, V.; Kraka, E.; Cremer, D. *Mol. Phys.* **2002**, *100*, 1771−1790.
(19) Cohen, A. J.; Mori-Sánchez, P.; Yang, W. *Science* **2008**, *321*, 792−794.
(20) Cramer, C. J.; Truhlar, D. G. *Phys. Chem. Chem. Phys.* **2009**, *11*, 10757−10816.
(21) Paier, J.; Marsman, M.; Kresse, G. *J. Chem. Phys.* **2007**, *127*, 024103.
(22) Johnson, B. G.; Gill, P. M. W.; Pople, J. A. *J. Chem. Phys.* **1993**, *98*, 5612−5626.
(23) Adamo, C.; Barone, V. *J. Chem. Phys.* **1999**, *110*, 6158−6170.
(24) Zhao, Y.; Truhlar, D. G. *Theor. Chem. Acc.* **2008**, *120*, 215−241.
(25) Zhao, Y.; Truhlar, D. G. *Acc. Chem. Res.* **2008**, *41*, 157−167.
(26) Tao, J.; Perdew, J. P.; Staroverov, V. N.; Scuseria, G. E. *Phys. Rev. Lett.* **2003**, *91*, 146401−4.
(27) Furche, F.; Perdew, J. P. *J. Chem. Phys.* **2006**, *124*, 044103.
(28) Zhao, Y.; Truhlar, D. G. *J. Phys. Chem. A* **2006**, *110*, 13126−13130.
(29) Stroppa, A.; Kresse, G. *New J. Phys.* **2008**, *10*, 063020.
(30) Koitz, R.; Soini, T. M.; Genest, A.; Trickey, S. B.; Rösch, N. *Int. J. Quantum Chem.* **2012**, *112*, 113−120.
(31) Koitz, R.; Soini, T. M.; Genest, A.; Trickey, S. B.; Rösch, N. *J. Chem. Phys.* **2012**, *137*, 034102.
(32) Braunstein, P.; Oro, L. A.; Raithby, P. R. *Metal Clusters in Chemistry*; Wiley: Weinheim, Germany, 1999.
(33) Heiz, U.; Landman, U. *Nanocatalysis*; Springer: Berlin, Heidelberg, 2007.
(34) Häberlen, O. D.; Chung, S.-C.; Stener, M.; Rösch, N. *J. Chem. Phys.* **1997**, *106*, 5189−5201.
(35) Krüger, S.; Vent, S.; Rösch, N. *Ber. Bunsen.-Phys. Chem.* **1997**, *101*, 1640−1643.
(36) Krüger, S.; Nörtemann, F.; Staufer, M.; Vent, S.; Rösch, N. *J. Chem. Phys.* **2001**, *115*, 2082−2087.
(37) Nava, P.; Sierka, M.; Ahlrichs, R. *Phys. Chem. Chem. Phys.* **2003**, *5*, 3372−3381.
(38) Yudanov, I. V.; Metzner, M.; Genest, A.; Rösch, N. *J. Phys. Chem. C* **2008**, *112*, 20269−20275.
(39) Yudanov, I. V.; Genest, A.; Rösch, N. *J. Cluster Sci.* **2011**, *22*, 433−448.
(40) Perdew, J.; Burke, K.; Ernzerhof, M. *Phys. Rev. Lett.* **1996**, *77*, 3865−3868.
(41) Staroverov, V. N.; Scuseria, G. E.; Tao, J.; Perdew, J. P. *J. Chem. Phys.* **2003**, *119*, 12129−12137.
(42) Zhao, Y.; Truhlar, D. G. *J. Chem. Phys.* **2006**, *125*, 194101.
(43) Dunlap, B.; Rösch, N. *Adv. Quantum Chem.* **1990**, *21*, 317−339.

(44) Belling, T.; Grauschopf, T.; Krüger, S.; Nörtemann, F.; Staufer, M.; Mayer, M.; Nasluzov, V. A.; Birkenheuer, U.; Hu, A.; Matveev, A. V.; Shor, A. V.; Fuchs-Rohr, M. S. K.; Neyman, K. M.; Ganyushin, D. I.; Kerdcharoen, T.; Woiterski, A.; Majumder, S.; Gordienko, A. B.; Huix i Rotllant, M.; Ramakrishnan, R.; Dixit, G.; Nikodem, A.; Soini, T. M.; Roderus, M.; Rösch, N. *ParaGauss, Version 4.0*; 2012.
(45) Flocke, N.; Lotrich, V. *J. Comput. Chem.* **2008**, *29*, 2722−2736.
(46) Nikodem, A.; Matveev, A. V.; Soini, T. M.; Rösch, N. *Int. J. Quantum Chem.* **2014**, *114*, 813−822.
(47) Weigend, F.; Ahlrichs, R. *Phys. Chem. Chem. Phys.* **2005**, *7*, 3297−3305.
(48) Andrae, D.; Häußermann, U.; Dolg, M.; Stoll, H.; Preuß, H. *Theor. Chim. Acta* **1990**, *77*, 123−141.
(49) Dunlap, B. I.; Rösch, N.; Trickey, S. B. *Mol. Phys.* **2010**, *108*, 3167−3180.
(50) Eichkorn, K.; Treutler, O.; Öhm, H.; Häser, M.; Ahlrichs, R. *Chem. Phys. Lett.* **1995**, *240*, 283−290.
(51) Eichkorn, K.; Weigend, F.; Treutler, O.; Ahlrichs, R. *Theor. Chem. Acc.* **1997**, *97*, 119−124.
(52) Lebedev, V. I. *Zh. Vychisl. Mat. Mat. Fiz.* **1975**, *15*, 48−54.
(53) Lebedev, V. I. *Zh. Vychisl. Mat. Mat. Fiz.* **1976**, *16*, 293−306.
(54) Becke, A. D. *J. Chem. Phys.* **1988**, *88*, 2547−2553.
(55) Häser, M.; Ahlrichs, R. *J. Comput. Chem.* **1989**, *10*, 104−111.
(56) Pulay, P. *Chem. Phys. Lett.* **1980**, *73*, 393−398.
(57) Marchal, R.; Yudanov, I. V.; Matveev, A. V.; Rösch, N. *Chem. Phys. Lett.* **2013**, *578*, 92−96.
(58) Bitzek, E.; Koskinen, P.; Gähler, F.; Moseler, M.; Gumbsch, P. *Phys. Rev. Lett.* **2006**, *97*, 170201.
(59) Nikodem, A.; Matveev, A. V.; Chaffey-Millar, H.; Soini, T. M.; Rösch, N. *ParaTools, Version 2*; 2012.
(60) Pacchioni, G.; Chung, S.-C.; Krüger, S.; Rösch, R. *Chem. Phys.* **1994**, *184*, 125−137.
(61) Wang, L.-L.; Johnson, D. D. *Phys. Rev. B* **2007**, *75*, 235405.
(62) Zhang, M.; Fournier, R. *Phys. Rev. A* **2009**, *79*, 043203.
(63) Drake, G. *Atomic, Molecular, & Optical Physics Handbook*. American Institute of Physics: Woodbury, NY, 1996.
(64) Warren, K. *J. Phys. Chem.* **1973**, *77*, 1681−1686.
(65) Alonso, J. A. *Chem. Rev.* **2000**, *100*, 637−677.
(66) Yudanov, I. V.; Genest, A.; Schauermann, S.; Freund, H.-J.; Rösch, N. *Nano Lett.* **2012**, *12*, 2134−2149.
(67) Taylor, A. *J. Inst. Metals* **1950**, *77*, 585.
(68) Rao, C. N.; Rao, K. K. *Can. J. Phys.* **1964**, *42*, 1336−1342.
(69) Waseda, Y.; Hirata, K.; Ohtani, M. *High Temp.−High Pressures* **1975**, *7*, 221−226.
(70) Janthon, P.; Luo, S.; Kozlov, S. M.; Viñes, F.; Limtrakul, J.; Truhlar, D. G.; Illas, F. *J. Chem. Theory Comput.* **2014**, *10*, 3832−3839 (DOI: 10.1021/ct500532v).
(71) Lejaeghere, K.; Van Speybroeck, V.; Van Oost, G.; Cottenier, S. *Crit. Rev. Solid State Mater. Sci.* **2014**, *39*, 1−24.
(72) Schumm, R. H.; Wagman, D. D.; Bailey, S.; Evans, W. H.; Parker, V. B. *Technical Notes 270-1 to 270-8*; National Bureau of Standards, Gaithersburg, MD, 1973.
(73) Kittel, C. *Introduction to Solid State Physics*, 8th Edition; Wiley: New York, 2004.
(74) Chase, M. W.; Davies, C. A.; Downey, J. R.; Frurip, D. J.; McDonald, R. A.; Syverud, A. N. *J. Phys. Chem. Ref. Data* **1985**, *14* (Suppl. 1).
(75) Zhao, Y.; Truhlar, D. G. *J. Chem. Phys.* **2006**, *124*, 224105.
(76) Seemüller, T. J. *Density Functional Studies on Properties of Nickel Clusters and Their Scaling with Cluster Size*; Diploma Thesis; Technische Universität München, München, Germany, 2000.
(77) Perdew, J.; Ruzsinszky, A.; Constantin, L. A.; Sun, J.; Csonka, G. I. *J. Chem. Theory Comput.* **2009**, *5*, 902−908.
(78) Cohen, A. J.; Mori-Sánchez, P.; Yang, W. *Chem. Rev.* **2012**, *112*, 289−320.
(79) Apsel, S. E.; Emmert, J. W.; Deng, J.; Bloomfield, A. *Phys. Rev. Lett.* **1996**, *76*, 1441−1444.
(80) Häberlen, O. D.; Chung, S.-C.; Rösch, N. *Ber. Bunsen.−Phys. Chem.* **1994**, *98*, 882−885.
(81) Riviere, J. C. Work Function: Measurements and Results. In *Solid State Surface Science*; Green, M., Ed.; Marcel Dekker: New York, 1969.
(82) Michaelson, H. B. *J. Appl. Phys.* **1977**, *48*, 4729−4733.
(83) Hölzl, J.; Schulte, F. K. Work Functions of Metals. In *Solid Surface Physics*; Höhler, G., Ed.; Springer: Berlin, 1979.
(84) Averill, F. W.; Painter, G. S. *Phys. Rev. B* **1992**, *46*, 2498−2502.
(85) Dunlap, B.; Mei, W. N. *J. Chem. Phys.* **1983**, *78*, 4997−5003.
(86) Chai, J.-D. *J. Chem. Phys.* **2012**, *136*, 154104.
(87) Monkhorst, H. J. *Phys. Rev. B* **1979**, *20*, 1504−1513.